MC Study of $K_L \to \pi^0 \nu \bar{\nu}$ Experiment at J-PARC B-line

Eiichi Tanaka

High Energy Physics Group

Department of Physics at Osaka University

March 26, 2004

Abstract

$K_L \to \pi^0\nu\bar{\nu}$ is very good probe to measure η which is an imaginary component in the CKM matrix that describes CP violation. We studied a new experiment to collect $K_L \to \pi^0\nu\bar{\nu}$ decays with a hermetic calorimeter at a new 50 GeV/c proton accelerator at J-PARC.

We found that we can collect 150 events in 3 years of running at 10% of the full accelerator intensity. The signal to background ratio is 1.1. With this statistics, we can measure η to within 6%.

Acknowledgement

I would like to thank T.Hara, M.Yamaga, K.Sumisawa and K.Hara for their invaluable advice on physics and experimental technique.

My special thanks go to K.Kotera, K.Sakashita, Y.Ikemoto, Y.Shibata, S.Komatsu, N.Nishi who gave me invaluable advice as members of this experiment. I enjoyed having many chats with them in my research life.

I also owe a lot to the members of the Yamanaka Taku Group at Osaka University for the good companionship and encouragement T.Houjo, H.Miyake, N.Hayama, have given me great deal of help proceed my research. I would like to thank S.Tsuzuki and N.Sugimoto. Their help and support for my research life must also be mentioned here.

Finally, I would like to thank Taku Yamanaka. He taught me physics, experimental technique, analysis and more. I am sure this thesis did not exist without his help and advice. Even my interest in high energy physics may come from him. I had a wonderful time with him and enjoyed a lot of talks about not only physics but also natural science, computer, and life.

Contents

List of Figures

List of Tables

Chapter 1

Introduction

The existence of symmetry principles in physics had been speculated as a manifestation of underlying beauty of order of the universe. From Newtonian mechanics to quantum mechanics, symmetry principles, connected with conservation laws, have provided us economical but elegant ways of looking at the nature. The law of left-right symmetry, associated with parity conservation, and invariance in charge conjugation operation, the two discrete symmetry laws which gained importance in quantum mechanics, had also been assumed to hold in subatomic world of physics. In this context, the breakdown of the combination of charge and parity symmetry in kaon decay, following parity violation discovered in weak interactions, had given us great impact on our view of the nature. At the same time, however, the discovery opened our eyes toward a new framework of physics. Afterwards, efforts have been paid to establish a model which incorporates the CP violation.

After about three decades since the CP breaking observation, so called the Standard Model has become believed to be the most probable candidate for the full description of elementary particle physics. Recent attention has been focused upon the complete determination of the parameters introduced in this scheme. In this respect, the rare kaon decay, $K_L \to \pi^0\nu\bar{\nu}$, has gained a key role for the determination of the parameters. We will describe the underlying physics and the purpose, overview of this study in this chapter.

1.1 Physics Interest in $K_L \to \pi^0\nu\bar{\nu}$

1.1.1 CP Violation

The combination of charge conjugation and parity transformation changes K^0 into $\bar{K}^0$, and vice versa:

$$CP|K^0\rangle = |\bar{K}^0\rangle\,, \tag{1.1}$$

$$CP|\bar{K}^0\rangle = |K^0\rangle\,. \tag{1.2}$$

(We use a conventional phase definition, and currently neglect the small effect of CP violation.)

The eigenvalues and eigenstates of CP are described as:

$$|K_1\rangle = \frac{1}{\sqrt{2}}\left[|K^0\rangle + |\bar{K^0}\rangle\right] \qquad (CP = +1)\,, \tag{1.3}$$

$$|K_2\rangle = \frac{1}{\sqrt{2}}\left[|K^0\rangle - |\bar{K^0}\rangle\right] \qquad (CP = -1)\,. \tag{1.4}$$

K_2 is the longer-lived kaons, whose lifetime is 5.2×10^{-8} seconds, and K_1 is the shorter-lived kaons, whose lifetime is 0.89×10^{-10} seconds. It had been believed from CP consistency that $|K_2\rangle$ decays to the three pions, which form a CP odd state, while $|K_1\rangle$ decays to two pions in a CP even state.

In 1964, Cronin and Fitch, *et al.*, observed that the longer-lived kaons decayed to two pions [1]. This suggests that CP odd long-lived kaons, K_L, decays into CP even mode, and CP is not conserved in this decay.

This phenomenon can be explained if K_L is actually composed not only of $|K_2\rangle$ but also with a slight mixture of $|K_1\rangle$:

$$|K_L\rangle = \frac{1}{\sqrt{1+\epsilon^2}}\left[|K_2\rangle + \epsilon|K_1\rangle\right]\,, \tag{1.5}$$

and K_1 decays to two pions. Such a mechanism for causing K_L to decay to two pions is called indirect CP violation. However, CP can be violated if K_2 in equation (1.5) decays to two π^0's. If K_2 directly decays to two pions, we can say that the CP is directly violated.

1.1.2 CKM parameter η

Currently, the powerful framework to explain CP violation is the Standard Model, which incorporates electromagnetic, weak, and strong interactions into a single scheme. It has a mechanism to introduce CP violation, including the direct CP violation.

In the Standard Model picture, direct CP violation is connected to the framework of quark mixing presented by Cabbibo, Koboyashi, and Maskawa [2]. In this theory, direct CP violation stems from the consequence of a three generation model.

The charged current in weak interaction can be written as:

$$J^\mu = \begin{pmatrix} \bar{u} & \bar{c} & \bar{t} \end{pmatrix} \frac{\gamma^\mu(1-\gamma^5)}{2} U \begin{pmatrix} d \\ s \\ b \end{pmatrix}. \tag{1.6}$$

The matrix U, introduced by Kobayashi and Maskawa, tells us the coupling of up and down type quarks:

$$U = \begin{pmatrix} V_{ud} & V_{us} & V_{ub} \\ V_{cd} & V_{cs} & V_{cb} \\ V_{td} & V_{ts} & V_{tb} \end{pmatrix} . \tag{1.7}$$

The 3×3 unitary matrix U can be represented by 4 parameters, with 5 arbitrary phases left aside. The 4 parameters, 3 are real parameters and 1 is a complex phase factor which accounts for the CP violation.

Wolfenstein parameterized the matrix components as follows [3]:

$$U = \begin{pmatrix} 1 - \frac{\lambda^2}{2} & \lambda & A\lambda^3(\rho - i\eta) \\ -\lambda & 1 - \frac{\lambda^2}{2} & A\lambda^2 \\ A\lambda^3(1 - \rho - i\eta) & -A\lambda^2 & 1 \end{pmatrix} . \tag{1.8}$$

The η parameter accounts for the CP violation, and the determination of the η parameter is one of the primary goals of particle physics of today. As we will see, measurement of the branching ratio of rare CP violating decays can determine the value of η.

1.1.3 Decay of $K_L \to \pi^0 \nu\bar{\nu}$

The rare decay $K_L \to \pi^0 \nu\bar{\nu}$ is a good window to determine the η parameter. As shown in Fig. 1.1, this decay is governed by short-distance transition current and occurs almost entirely from the direct CP violation, as described below.

The amplitude for $K_L \to \pi^0 \nu\bar{\nu}$ can be written as

$$A(K_L \to \pi^0 \nu\bar{\nu}) = \frac{1}{\sqrt{1+\epsilon^2}} \left[A(K_2 \to \pi^0 \nu\bar{\nu}) + \epsilon A(K_1 \to \pi^0 \nu\bar{\nu}) \right] , \tag{1.9}$$

or

$$A(K_L \to \pi^0 \nu\bar{\nu}) = \frac{1}{\sqrt{2(1+\epsilon^2)}} \left[(1+\epsilon) A(K^0 \to \pi^0 \nu\bar{\nu}) - (1-\epsilon) A(\bar{K^0} \to \pi^0 \nu\bar{\nu}) \right] , \tag{1.10}$$

using equations (1.3) and (1.4). Since top quark can be in an intermediate state(Fig. 1.1), this decay involves to the V_{td} and V_{ts}. Using the Wolfenstein's parameterization (1.8),

$$A(K_L \to \pi^0 \nu\bar{\nu}) \propto V_{td}^* V_{ts} - V_{ts}^* V_{td} \sim 2i\eta \, . \tag{1.11}$$

Thus, we can see that the branching ratio of $K_L \to \pi^0 \nu\bar{\nu}$ is proportional to η^2, and its measurement determines the η parameter.

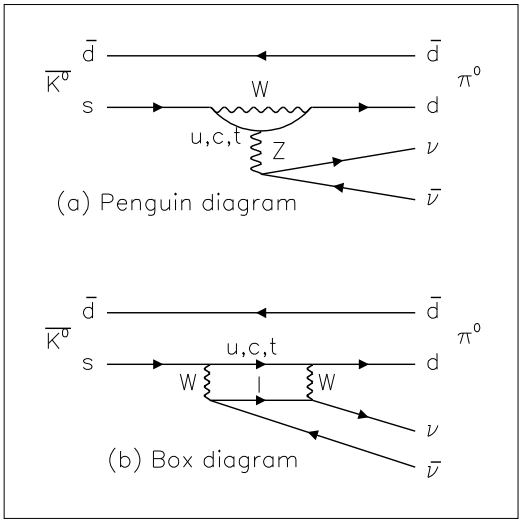

Figure 1.1: The Z penguin and W-box diagrams which contribute to the decay $K_L \to \pi^0\nu\bar{\nu}$

The branching ratio can be calculated [4, 5] as

$$BR(K_L \to \pi^0\nu\bar{\nu}) = 1.94 \times 10^{-10}\eta^2 A^4 \chi^2(x) \tag{1.12}$$

where $x = m_t/m_W$, $\chi \sim x^{1.2}$, and A is a CKM parameter in Wolfenstien parameterization (equation 1.8). The theoretical estimate of this branching ratio is $\cong 3.0 \times 10^{-11}$ based on the current knowledge of CKM parameters [4, 5]. Due to the uncertainties on the CKM parameters, these predictions still contain an error of $\cong 2 \times 10^{-11}$. The best published limit the $K_L \to \pi^0\nu\bar{\nu}$ decay is 5.9×10^{-7} (90%CL) from E799-I at Fermi National Accelerator Laboratory (FNAL)[6]. The theoretical uncertainty on the relation between $BR(\ K_L \to \pi^0\nu\bar{\nu}\ )$ and η, that is the uncertainty in $A^4\chi^2(x)$ in equation (1.12), has a magnitude of a few percent[4]. Therefore, by measuring the branching ratio of $K_L \to \pi^0\nu\bar{\nu}$, we can directly determine the CKM parameter η with a high accuracy.

1.2 $K_L \to \pi^0\nu\bar{\nu}$ experiment

In this section, we will describe the experimental challenges for detecting $K_L \to \pi^0\nu\bar{\nu}$ and possible kinematic variables that we could use. Our goal is to measure η within a precision of 10% by collecting more than 100 $K_L \to \pi^0\nu\bar{\nu}$ events.

As we have seen, $K_L \to \pi^0\nu\bar{\nu}$ has a very small branching ratio. The number of observed $K_L \to \pi^0\nu\bar{\nu}$ events is:

$$N_{evt} = N_{K_{decay}} \times BR \times A \tag{1.13}$$

where $N_{K_{decay}}$ is number of K_L's which decay in a fiducial region, BR is the branching ratio of $K_L \to \pi^0\nu\bar{\nu}$, and A is a detector acceptance. Therefore, in order to collect large number of events, we need a high K_L decay rate, and a detector with a large acceptance.

Since almost 99 % of π^0's decay into two γ's, the detection of $K_L \to \pi^0\nu\bar{\nu}$ means finding 2γ's originating from a π^0 decay. This raises some difficulties for observing $K_L \to \pi^0\nu\bar{\nu}$.

First difficulty is the measurement of the vertex position. Orthodox photon detectors can only measure energy and position of gammas, but cannot measure the direction of gamma. However, if we can measure the direction or the timing of gamma with a good accuracy, we can apply more constraints to measure the decay vertex.

Therefore we should find out whether a detector with current technology which measure gamma's direction and time difference is effective or not.

Second difficulty is the existence of many difficult backgrounds sources. The decay modes which can be background are $K_L \to \pi^0\pi^0$, $K_L \to \pi^0\pi^0\pi^0$, $K_L \to \gamma\gamma$, $K_L \to \pi^0\gamma\gamma$, $\Lambda \to n\pi^0$, etc.. Of these backgrounds, the dominant and the most severe background is $K_L \to \pi^0\pi^0 \to 4\gamma$(BR=$9.36\times10^{-4}$) where two gammas are missed. To avoid missing the gammas, we need a hermetic coverage around the K_L decay region. In addition, the photon detector should have a low detection inefficiency. This inefficiency is a strong function of the energy of the gamma, and is lower for high energy gammas. The inefficiency also depends on the energy threshold of photon detectors.

Moreover, there are two kinds of backgrounds from $K_L \to \pi^0\pi^0$; (a)even pair background which is caused by missing two gammas originating from the same pion, and (b)odd pair background caused by missing two photons from different pions. Of these backgrounds, even pair background has a similar property as the signal because the observed two gammas come from one pion. Therefore, the suppression of even pair background is more difficult than that of odd pair background. To suppress even pair background, we should measure all kinematics of this decay, so E_{K_L} is an important variable. Therefore, we should find out the effect of measuring E_{K_L}.

Now, various experiments are approaching these problems with different methods.

For example, BNL(Brookhaben National Laboratory) is proposing to completely measure the kinematics of the gammas including position, angle, energy, and the time of flight(TOF) of K_L to measure the K_L momentum, and reconstruct π^0 momentum in the K_L center of mass system. In order to measure the K_L momentum by TOF, they plan to use a K_L beam with low momentum around 700 MeV/c. In addition, they are planning to use photon veto detectors surrounding the decay region. The sensitivity is 6×10^{-13} in 9000 hours.

At KEK(High Energy Accelerator Research Organization in Japan), E391 uses typically 2 GeV/c K_L beam. This beam energy is selected to avoid the background due to hyperons which are potential problems at high K_L energy, but to keep the gamma's energy high enough to achieve a good veto efficiency. The detector is surrounded by a hermetic veto counter to reduce the $K_L \to \pi^0\pi^0$ background. The sensitivity is 3.0 $\times 10^{-10}$.

1.3 Motivation and Overview

In future, E391 will move to J-PARC(Japan Proton Accelerator Research Complex) to collect more than 100 $K_L \to \pi^0\nu\bar{\nu}$ events. J-PARC is a new accelerator project in Japan which produces MW-class high power proton beam. B-line is one of the J-PARC beam line for K_L and hadron experiments. B-line is suitable for the $K_L \to \pi^0\nu\bar{\nu}$ experiment because of its high energy (50GeV) and high intensity (3.3×10^{14} proton per pulse) beam which can produce many high energy K_L's.

The goal of this study is to design an experiment to measure the η with a precision less than 10% by collecting more than 100 $K_L \to \pi^0\nu\bar{\nu}$ events.

We will study a $K_L \to \pi^0\nu\bar{\nu}$ experiment for B-line using Monte Carlo. Our design principle is as follows.

- Use high momentum K_L to reduce the gammas inefficiency.
- Cover the decay region with a hermetic calorimeter and achieve a high acceptance.
- Study what other information, such as direction of gamma, timing of gamma or energy of K_L are useful for the experiment.

In this study, we considered $K_L \to \pi^0\pi^0$ as background mainly, because this background is expected to be dominant and difficult to suppress.

In the next chapter, we will simulate target region which produce secondary particle with 50 GeV/c proton. In Chapter 3, we will simulate the region between target and fiducial volume, which makes beam clean and collimate for K_L beam line. In Chapter 4, we will simulate fiducial region with above conditions. In Chapter 5, we will simulate fiducial region with improved conditions. In Chapter 6, we will show results and conclusion of this study.

Chapter 2

Target region

To get the best K_L beam for $K_L \to \pi^0\nu\bar{\nu}$, we first studied target section. The 50GeV/c protons from the J-PARC accelerator hit the target to produce a neutral beam. Large K_L yield and high momentum K_L beam are advantageous for collecting $K_L \to \pi^0\nu\bar{\nu}$. The rate of neutrons should be suppressed for $K_L \to \pi^0\nu\bar{\nu}$ experiment because neutron can cause background source, such as by producing π^0 in the residual gas.

2.1 Condition and Geometry

In this simulation, we bombarded 50 GeV/c primary protons on various production targets to study the momentum spectrum and the yield of K_L, neutron and other secondary particles. The target was assumed to be a 1 interaction length(λ_I) long, 0.6cm$^{\phi}$ cylinder. The proton beam with 0 radius was injected at the center of the target along the axis. We studied four different target materials, Be, Al, Ni and Pt. The threshold energy for tracing in the simulation was set to be 100keV. The number of generated protons was 5×10^5 for each target material. We collected secondary particles at 1cm away from the target surface surrounding 4π solid angle.

2.2 Material dependence

In this section, we will compare the momentum spectrum and the rates for different target materials.

Figure 2.1 shows polar angle distribution of K_L and neutron for each target material. We can see that K_L yield does not depend strongly on the target materials. On the other hand, the neutron yield is higher for high density materials, such as Pt.

Figure2.2 shows the polar angle distribution of neutron/K_L ratio(n/K_L ratio). The n/K_L ratio is minimum at 3° to 4°, independent of materials.

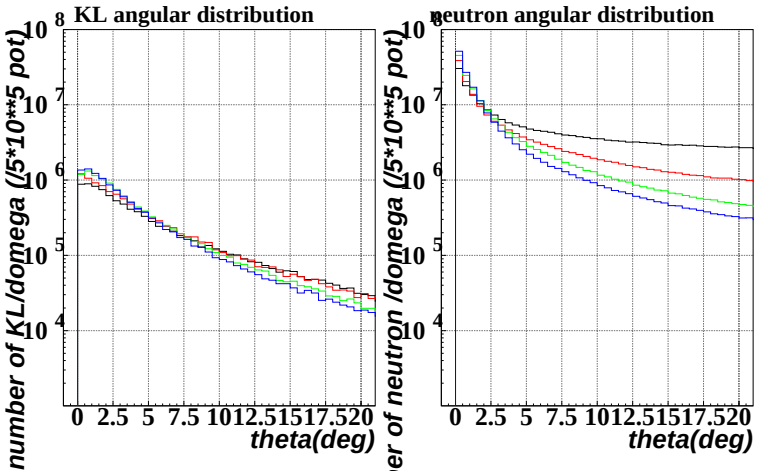

Figure 2.1: These plots show polar angle distributions of K_L's(left) and neutrons(right) for target materials; Pt(black), Ni(red), Al(green) and Be(blue).

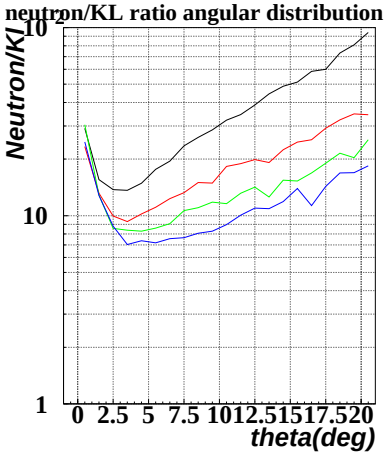

Figure 2.2: The neutron/K_L ratio as a function of extraction angle for different target materials; Pt(black), Ni(red), Al(green), Be(blue).

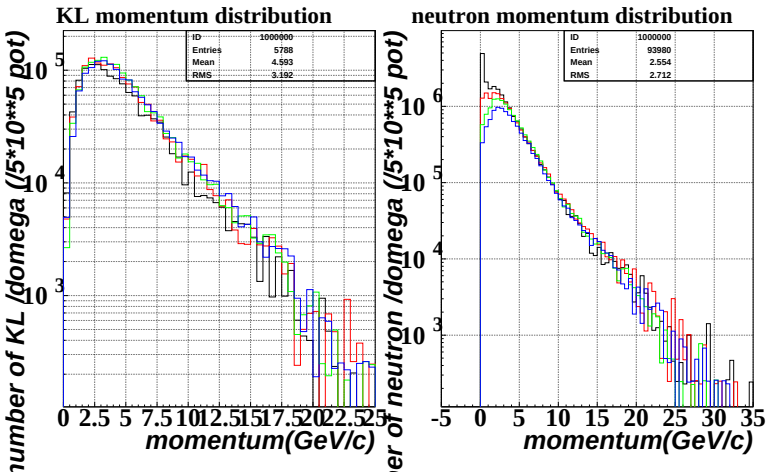

Figure 2.3: The momentum distribution of emitted between 4° to 6° from the proton beam axis. The same color code is used as in Fig.2.2.

Figure2.3 shows momentum distribution of K_L's and neutrons emitted in the polar angle between 4° and 6°. The momentum distribution of K_L does not depend on the target materials. However, low energy neutrons are produced in heavy materials. These low momentum neutrons do not contribute to the $K_L \to \pi^0\nu\bar{\nu}$ background, since their momentum is below 800 MeV/c which is the π^0 production threshold.

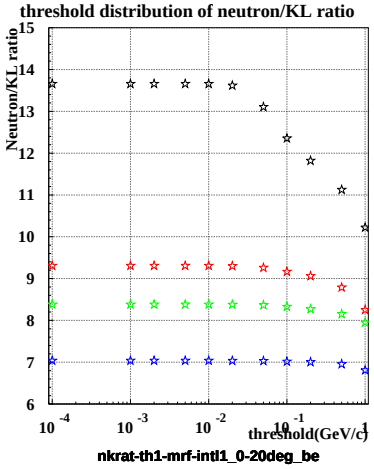

Figure 2.4: This plot shows threshold energy distribution of neutron/K_L ratio at 4° for each target materials. The same color code is used as in Fig.2.2.

Figure 2.4 shows the n/K_L ratio for particles emitted at 4° above a given momentum

threshold. Above 800 MeV/c, the n/K_L ratio of Pt is 1.5 times larger than Be.

2.3 Target thickness dependence

Next, we vary the thickness of the targets and compare the K_L and neutron yields.

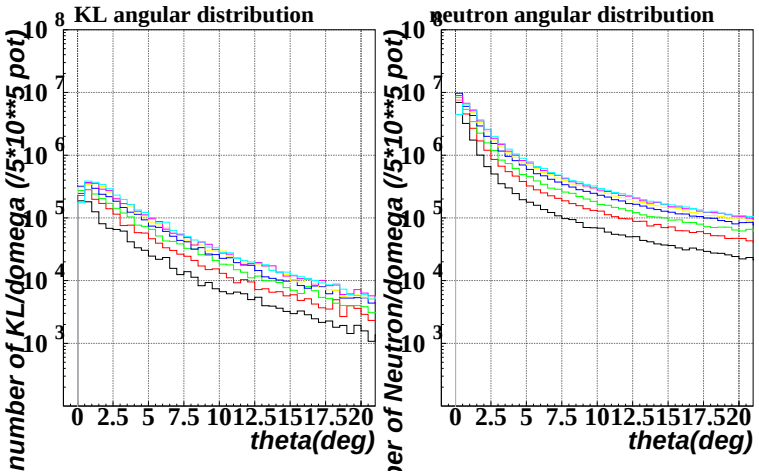

Figure 2.5: The polar angle distribution of K_L(left) and neutron(right) for different target thicknesses; $0.36\lambda_I$(black), $0.7\lambda_I$(red), $1.0\lambda_I$(green), $1.5\lambda_I$(blue), $2.0\lambda_I$(yellow), $2.5\lambda_I$(pink), and $3.0\lambda_I$(light-blue).

Figure 2.5 shows the polar angle distribution of K_L and neutron for different Be thicknesses. Although the yield increases for a thicker target, they reach a plateau beyond $3\lambda_I$.

2.4 Summary

In this target simulation, we have studied secondary K_L and neutron particles. We decided to use a 1 λ_I Pt target with 4° targeting angle. Although its n/K_L ratio is higher than Be, the difference is due to low momentum neutron, and thus will not contribute to the background. In addition, it is important to keep the target size small for making a pencil beam, as will see in later chapters. The K_L yield at 4° extraction angle is $8\times10^4 K_L/(5\times10^5$ proton$)/d\Omega$. The average momentum of K_L at the target is 4.5GeV/c. The n/K_L ratio is 11 above 0.8 GeV/c.

Chapter 3

Neutral beam line

In this chapter, we will design the neutral beamline. The purpose of the beamline is to bring a well collimated, high purity K_L beam to the downstream detector. We will study how to reduce the number of neutrons, photons, and Λ's relative to the number of K_L's.

3.1 Condition and Geometry

First, let us define our coordinate system. We set the origin at the production target, and choose the Z axis along the neutral beam line.

In this chapter, for the neutral beamline simulation, we assumed a 0.6cm$^{\phi}$ proton beam hitting a 0.6cm$^{\phi}$ and 1 λ_I (40.7cm) long Be target. We used Be instead of Pt simply because it was faster to simulate. The threshold energy in the simulation was set to 1 MeV. We collected secondary particles whose extraction angle was 4° at 1m from the target.

We then transported the collected particles down the beamline. The beamline consists of three elements. First is magnet to sweep out charged particles. Second is absorber to reduce the n/K_L ratio. The last collimates the beam. To save the CPU time, we did not simulate interactions in the collimator material. Instead, we simply considered neutral particles which entered the collimator. The beam size was set to 1 mrad in a half-cone angle.

3.1.1 Estimation of proton yield

We assumed to use 10% of the full intensity of J-PARC. The beam cycle time is 3.4 sec. We assumed 3 years of running, where 1 year is assumed to be 1×10^7sec. In this running time, we get a total of 3×10^{20} protons.

3.2 Absorber effect

As an absorber, we chose two materials. One was Be to reduce the number of neutrons. The other was Pb to reduce the number of gammas. This difference of materials is derived from a ratio of an interaction length to a radiation length; the ratio is low for Be, and high for Pb.

We carried out the simulation of the beam line absorber materials. We set a 0.75 λ_I long Be followed by 9 X_0 long Pb as a absorbers at 5m downstream the target. K_L, neutron and gammas were collected at 15m downstream of the target. The momentum distribution of K_L, neutron and gamma are shown in Fig.3.2, and for a comparison, those without the absorber are shown in Fig.3.1.

With this absorber set, the n/K_L ratio was reduced from 8 to 4. The γ/K_L ratio did not change with the absorber, but the average gamma momentum was lowered from 2.1GeV/c to 0.08GeV/c.

3.3 Residual Λ

In this simulation, the number of Λ was 965 at 5m behind the target for 7×10^9 protons. This corresponds to 1×10^{13} Λ for 3×10^{20} protons in 3 years of beam time.

The momentum distribution of Λ at 5m downstream of the target is shown in Fig.3.3.

If Λ survives up to the decay fiducial region, the $\Lambda \to \pi^0 n$ decay with a branching ratio of 35.8% is a possible background source for $\pi^0 + nothing$. However, most of Λ's decay before the fiducial region due to short life time, $c\tau = 7.89$cm. The background from Λ can be suppressed if we place the decay region farther downstream.

The number of Λ is shown in Fig.3.4 as a function of a decay point.

The number of Λ at Z = 50m is estimated to be $3.3\times10^2/(3 \times 10^{20}$ protons). The maximum transverse momentum of the π^0 in the $\Lambda \to \pi^0 n$ decay is 104 MeV/c, which is lower than that of $K_L \to \pi^0\nu\bar{\nu}$ (231 Mev/c). The residual Λs background is further suppressed by a cut on the kinematics of the π^0, as described in Section 4.2.

3.4 Summary

In this chapter, we have studied the neutral beam line. In the following studies, we will use a 0.75 λ_I thick Be absorber and a 9 X_0 thick Pb absorber. We decided to place detectors at 50m from the target to suppress the number of Λ's. Within a 1.2 μstr cone at 4° off the proton beam axis, at Z = 50m, we expect $2.0\times10^{14} K_L$'s, 1.2×10^{15} neutrons, 1.1×10^{17} gammas, and 1.2 $\times10^3\Lambda$'s for 3×10^{20} protons on Be target.

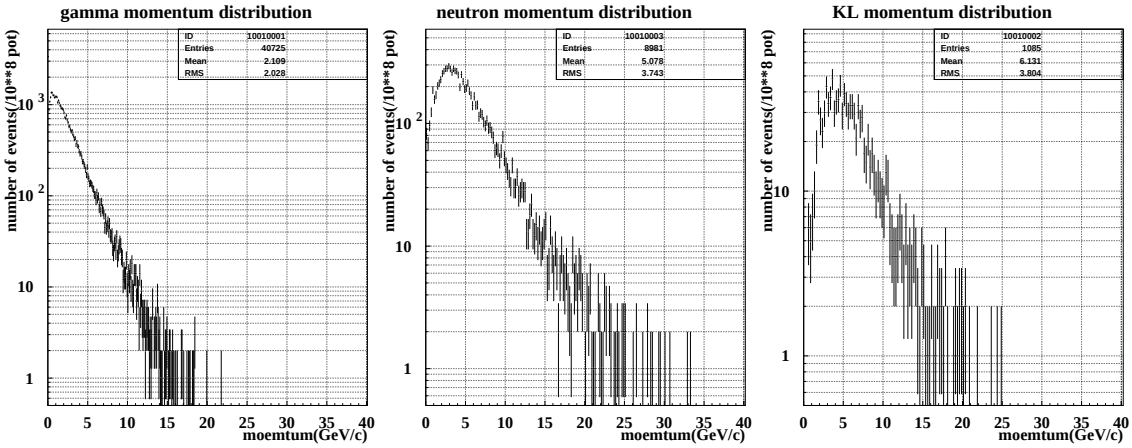

Figure 3.1: These momentum distributions of gamma(left),neutron(center),K_L(right) with no absorber.

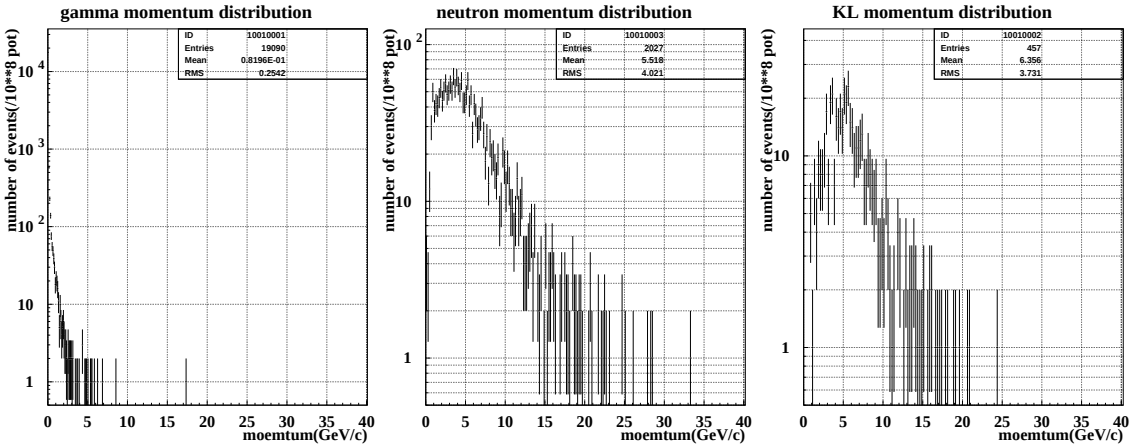

Figure 3.2: The momentum distributions of gamma(left),neutron(center),K_L(right) with a 0.75 λ_I long Be and a 9 X_0 long Pb absorber.

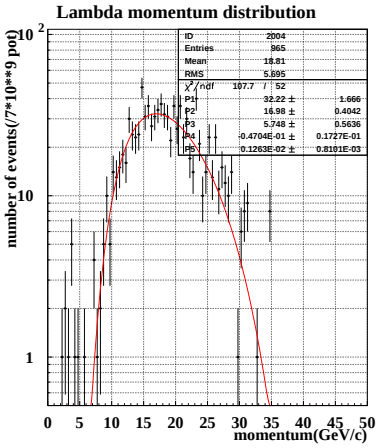

Figure 3.3: This plot shows the momentum distribution of Λ. the black points is MC data with error. the red line is the fitting for a asymmetry gaussian.

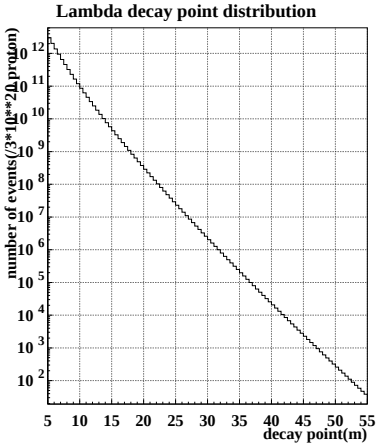

Figure 3.4: This plot shows Λ decay position. we calculated this line using the momentum distribution 3.3. the black line shows the decay point with all momentum data.

Chapter 4

Detector configuration and sensitivity on η

In this chapter, we will assume a simplified detector for the experiment, and study the signal and background acceptances. We will show the results on η's precision. First, we will use energy and hit position of gammas for reconstructing events. We will then study other measurements, such as incident angle, timing of gamma, and the time of flight(TOF) of K_L, would improve the experiment.

4.1 Condition and Geometry

In this section, we will explain basic conditions for the fiducial region in detail.

4.1.1 K_L beam

In this simulation, we assumed to use a 1 λ_I(8.8cm) long Pt target followed by 0.75λ_I long Be and 9X_0 long Pb absorbers.[1] K_L momentum spectrum at Z=20m which we used in this simulation is shown in Fig.4.1. We generated K_L within 1.2 μstr cone.

4.1.2 Detector Setup

The fiducial design which we used for the simulation is shown in Fig.4.2.

We decided to place the fiducial region starting at Z=50m, in order to reduce the number of Λ's to a manageable level. The length of the fiducial volume is 15m long. The fiducial region is surrounded by a cylindrical photon detector(Side Calorimeter) which is 15m long and 1m in radius. At Z=65m, we placed another photon detector(End

[1] Actually, we used the K_L momentum spectrum for Be target, because the spectrum was similar to Pt and the simulation of K_L production was far faster than Pt.

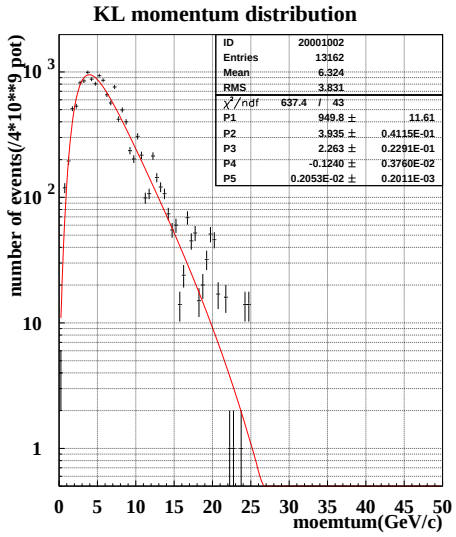

Figure 4.1: The momentum distribution of K_L at 20m. The black points show MC data. The red line shows an asymmetric gaussian used for fitting.

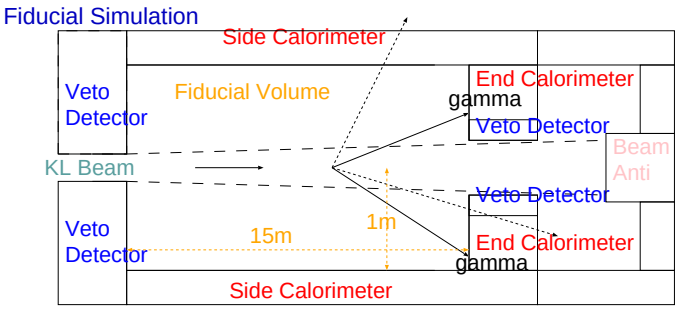

Figure 4.2: detector setup

Calorimeter). The end calorimeter had a 10.4cm$^{\phi}$ hole at the center to let the beam go through. The region within 30.4cm$^{\phi}$ was used as a veto detector, and its outside was used as a calorimeter. At Z=50m, a veto detector with a 6.2cm$^{\phi}$ hole at the center was placed. The region between the End calorimeter and Z=75.5m was covered by photon detector. At Z=75.5m, we placed a photon veto detector. to detect photons escaping from the beam hole of End Calorimeter.

4.1.3 Performance of photon counter

We assumed that the photon detectors have the following characteristics.

Resolution of photon counter

The detector measured the energy and position of gammas with finite resolutions. Here, we only smeared gamma's information in the calorimeter with Gaussian.

The energy resolution was assumed to be

$$\frac{\Delta E}{E} = \frac{9\%}{\sqrt{E}} \tag{4.1}$$

where E is energy of gamma in GeV, which is typical for lead/scintillator sandwich calorimeter.

The position resolution was assumed to be

$$\Delta X = \frac{0.5(cm)}{\sqrt{E(GeV)}}. \tag{4.2}$$

Inefficiency of photon counter

The detector was assumed to have an inefficiency of lead/scintillator sandwich sampling calorimeter.

This inefficiency is critical for $K_L \to \pi^0\nu\bar{\nu}$ experiment because missing 2γ events in $K_L \to \pi^0\pi^0$ is background. For the sampling calorimeter, the dominant components of inefficiencies are photo-nuclear interaction, sampling effect and punch through. In the following, we will briefly describe these mechanisms.

The photo-nuclear interaction is a reaction that an incident gamma is absorbed by the nucleus and this nucleus emits protons, neutrons, or photons. If the nucleus emits protons or high energy photon, it is easy to detect. On the other hand, if the nucleus emits only neutrons or low energy photons, it is difficult to detect, because neutrons have no charge and do not react by electro-magnetic interaction. In this case, the incident photon will not be detected.

Other inefficiency components are sampling effect and punch through. In the case of sampling calorimeters, if an incident photon deposits most of its energy into lead layers,

and deposits energy below a detection threshold into the scintillator, the photon will not be detected. This is called sampling effect. If a photon goes through the detector without reaction, the photon will not be detected. This is called punch through.

These three effects, have been measured or studied by MC simulation.[7]

Each inefficiency is a function of the energy threshold of the detector. The data was set to have a 5 MeV threshold for incident energy of gammas. In the following studies, we will assume that photon detectors have the inefficiency shown in Fig.4.3.

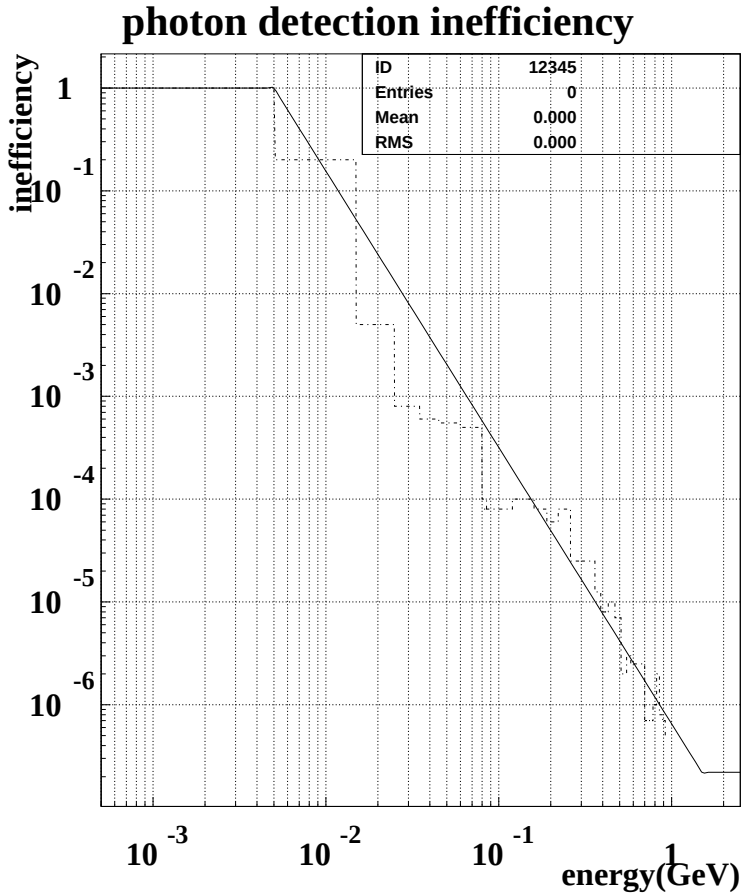

Figure 4.3: Photon detection inefficiency as a function of the photon energy for 1mm Pb/5mm Scintillator sampling calorimeters whose threshold is 5MeV. The dotted line is experimental data.[7] The solid line shows the inefficiency we assumed in the simulation.

At Z=75.5m, we placed a photon detector, but the region within 6.0 cm from the beam axis was assumed to be totally insensitive to photons, to be conservative because of high rate; 2.2×10^8 Hz neutrons and 2.5×10^7 Hz K_L.

4.1.4 event weight

With the photon inefficiency we described, the probability of missing 2 photons is extremely low. If we simply apply the inefficiency to each photon, most of the generated events would be rejected, and it will take too long to run simulation. In order to overcome this problem, we assigned a 'weight' to each event which is the probability for observing the event. For $K_L \to \pi^0\pi^0$, we considered all combinations of choosing two detected gammas from four gammas. For each combination, we assigned a weight as shown in Table 4.1.

Table 4.1: $K_L \to \pi^0\pi^0$ weight table. $\bar{\epsilon}(E_i)$ means an inefficiency of 'i'th gamma with E_i.

detected gammas energy	missing gammas energy	weight
E_1, E_2	E_3, E_4	$(1. - \bar{\epsilon}(E_1))(1 - \bar{\epsilon}(E_2))\bar{\epsilon}(E_3)\bar{\epsilon}(E_4)$
E_1, E_3	E_2, E_4	$(1. - \bar{\epsilon}(E_1))(1 - \bar{\epsilon}(E_3))\bar{\epsilon}(E_2)\bar{\epsilon}(E_4)$
E_1, E_4	E_2, E_3	$(1. - \bar{\epsilon}(E_1))(1 - \bar{\epsilon}(E_4))\bar{\epsilon}(E_2)\bar{\epsilon}(E_3)$
E_2, E_3	E_1, E_4	$(1. - \bar{\epsilon}(E_2))(1 - \bar{\epsilon}(E_3))\bar{\epsilon}(E_1)\bar{\epsilon}(E_4)$
E_2, E_4	E_1, E_3	$(1. - \bar{\epsilon}(E_2))(1 - \bar{\epsilon}(E_4))\bar{\epsilon}(E_1)\bar{\epsilon}(E_3)$
E_3, E_4	E_1, E_2	$(1. - \bar{\epsilon}(E_3))(1 - \bar{\epsilon}(E_4))\bar{\epsilon}(E_1)\bar{\epsilon}(E_2)$

In this simulation, we treated each combination as a separate event. Since the inefficiency is very small, these weights are far smaller than '1'.

4.2 Analysis using only energy and hit position of gammas

In this section, we will describe the analysis which only uses the gamma's energy and hit position in the calorimeter.

Reconstruction of decay vertex

First, we calculated the decay vertex position, by assuming that two detected gammas came from one π^0 on the Z axis. We can then calculate the angle between the two gammas, θ, by

$$cos\theta = 1 - \frac{M_{\pi^0}^2}{2E_{\gamma 1}E_{\gamma 2}} \tag{4.3}$$

where M_{π^0} is the mass of π^0, and $E_{\gamma 1}$ and $E_{\gamma 2}$ are the energies of two detected gammas. Using this θ and the gammas hit positions, we can calculate the decay position on the Z vertex. There can be however, two candidate decay positions, typically in the upstream and downstream of the detected position.

To describe this reason clearly, we will define three categories as the gammas hit pattern in the calorimeter. Category EE means that 2 photons were detected in the 'End calorimeter'. Category SS means that 2 photons were detected in the 'Side calorimeter'. Category ES means that one photon was detected in 'End calorimeter' and the other was detected in 'Side calorimeter'.

For category EE, we simply chose the vertex in upstream. For category SS and ES, although two candidate decay positions are possible, we chose the vertex in the upstream. This is because with the mean K_L momentum of 6.4 GeV/c, most of the gammas fly downstream. Note that this method gives the correct decay position only for the signal events and the even pair background events, but not for the odd pair background events.

Using this decay vertex position and the gamma's energies and hit positions, we can calculate the momentum of the two gamma's, and the transverse momentum(P_T) of the π^0.

cut criteria

In this section, we will introduce cut criteria. Before tuning the cuts on Z decay position and P_T, we applied the following cuts.

The energy of each gamma was required to be more than 100 MeV. The condition is important to ensure that the 2 gammas are detected with good energy and position resolutions. Also, this cut rejected events with $\cos\theta < 0$.

In order to suppress background from $K_L \to \gamma\gamma$ events, we introduce another kinematical variable, acoplanarity angle, which is defined as a supplement of angle spanned by the momentum vectors projected on a plane perpendicular to the beam axis. Most of $K_L \to \gamma\gamma$ events can be rejected by the transverse momentum cut because the 2 gammas from the $K_L \to \gamma\gamma$ decay have balanced P_T. However, P_T can become large if the energy of one gamma is mis-measured due to photonuclear-interaction in $K_L \to \gamma\gamma$ decay. In this simulation, we required acoplanarity angle $> 20^\circ$.

Next, we consider the following criteria to decide the cut regions for P_T and Z decay position.

First, we will decide the lower limit on the P_T of π^0 considering the background from Λ. As we said in the previous chapter, the Λ's remaining in the fiducial region can be background sources because they decay to $\pi^0 n$.

In our present setup, 3.3×10^2 Λ's decay in the fiducial region in 3 years. To estimate the number of Λ's background events, we generated 10^6 Λs using the momentum distribution shown in Fig.3.3, and analyzed their P_T of π^0s. The result is shown in Fig.4.4. We set a criteria that the Λ background events are less than 10 for each category; EE,

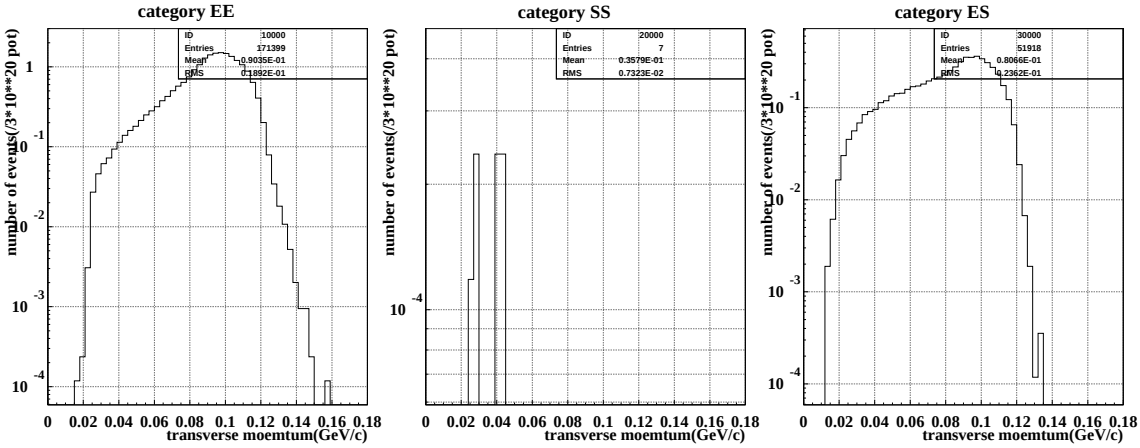

Figure 4.4: The distribution of Λ's transverse momentum for each hit category, EE(left), SS(center) and ES(right).

SS and ES. The lower cut on P_T was set to 117 MeV/c for category EE, and 90 MeV/c for category ES. No cut was necessary for category SS because none of the Λ decays had 2 gammas hitting the side, due to Λ's high momentum.

Next, the lower limit on Z decay position should be set away from the upstream end of the decay volume. Figure 4.5 show the difference between actual Z and the reconstructed Z vertex. The height of the distribution is lowered by > 2 orders of magnitude at 2m. Although we need more detailed studies, we required Z > 52 m.

estimation of η's precision

Here, we mentioned simulation condition. We generated 10^7 $K_L \to \pi^0\nu\bar{\nu}$ decays and 10^8 $K_L \to \pi^0\pi^0$ decays. We normalized these generated data to 2.5×10^{14} K_L at Z=20m which is estimated as K_L yield in a 3 years beam time.

The relative error on η is

$$\frac{\Delta\eta}{\eta} = \frac{1}{2}\frac{\Delta BR}{BR} \tag{4.4}$$

$$= \frac{1}{2}\frac{\sqrt{(S+N)}}{S}, \tag{4.5}$$

where BR is branching ratio of $K_L \to \pi^0\nu\bar{\nu}$, S is the number of signal events, and N is the number of background events. Here, we only consider statistical error. Consequently, the $\frac{\Delta\eta}{\eta}$ depends on the number of signal and background events, which depends on the signal region.

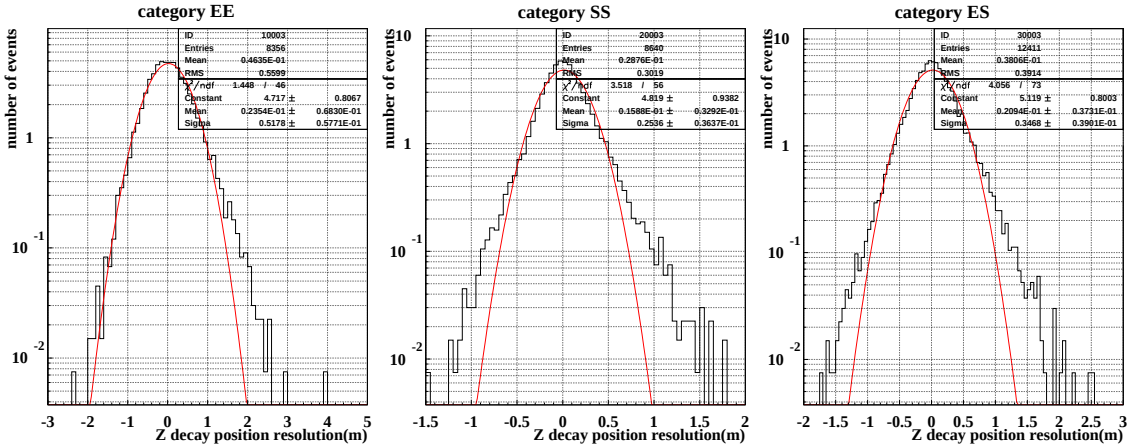

Figure 4.5: The resolution of Z decay position. for each hit category, EE(left), SS(center) and ES(right).

We made two-dimensional plot for P_T and Z for the signal, signal to background ratio and $\frac{\Delta\eta}{\eta}$. Figure 4.6 shows these results.

The distribution of P_T which has a broad peak around 190 MeV/c is a feature of $K_L \to \pi^0\nu\bar{\nu}$. We can see the difference between hit pattern categories. Here, we focus on $\frac{\Delta\eta}{\eta}$ to decide a cut region to minimize $\frac{\Delta\eta}{\eta}$. The cut result is shown in Table 4.2.

Table 4.2: cut table for analysis using only energy and hit position of gammas

	z minimum(m)	z maximum(m)	P_T minimum(GeV/c)	P_T maximum (GeV/c)
category EE	52.1	59.75	0.135	0.240
category SS	52.1	57.95	0.135	0.240
category ES	52.1	60.5	0.135	0.240

After the cut, we can get signal event, signal to background ratio, and $\frac{\Delta\eta}{\eta}$ for each hit category. The result is shown in Table 4.3.

Taking the difference of categories into consideration, we apply the error of the weighted average for calculating η's precision, and obtained $\frac{\Delta\eta}{\eta} = 6.4\%$.

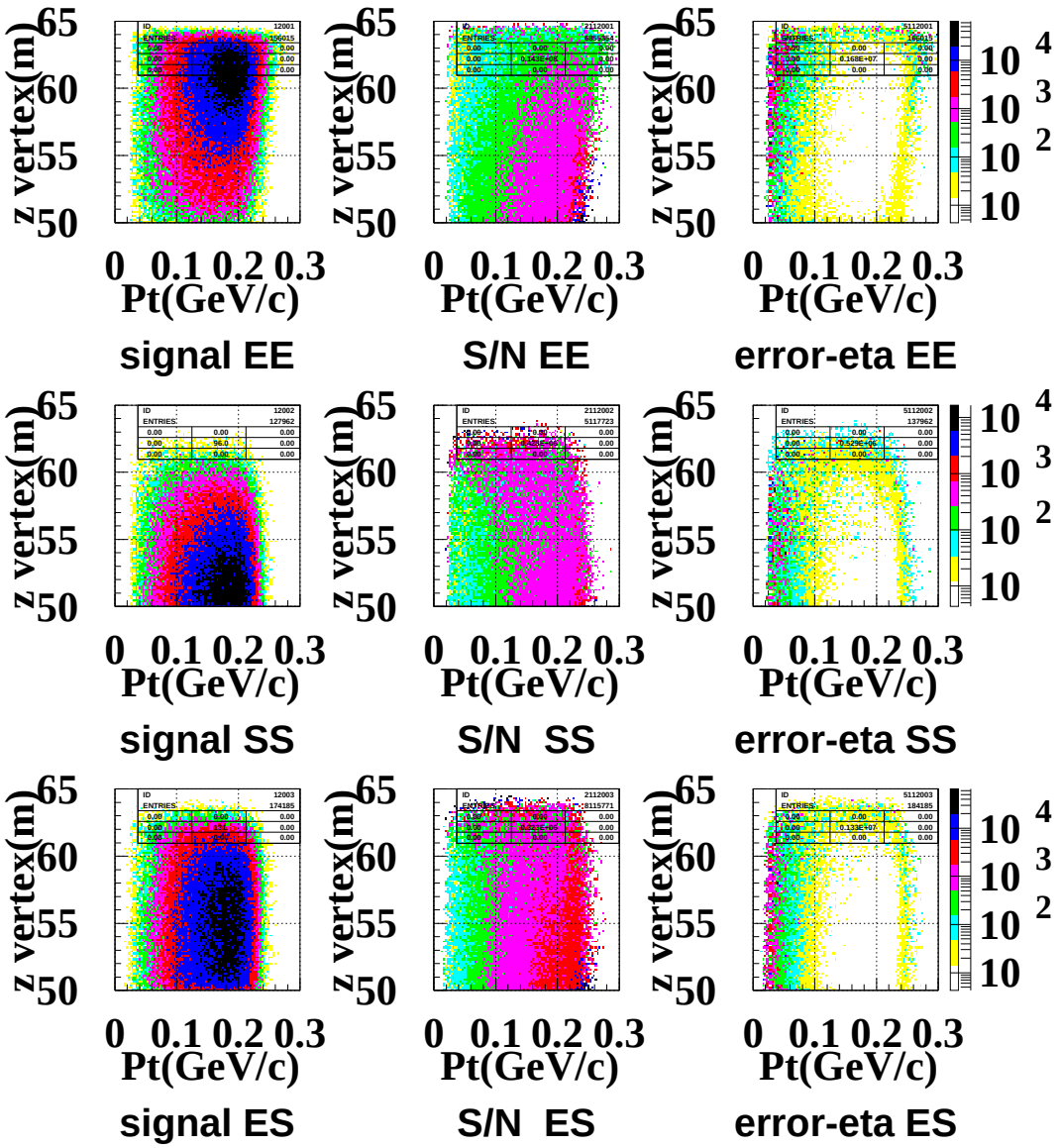

Figure 4.6: kinematical signature with analysis using only energy and hit position of gammas. left column shows number of signal events

Table 4.3: The number of signal events, signal to background ratio, $\frac{\Delta\eta}{\eta}$ with analysis using only energy and hit position of gammas

	signal	signal to background ratio	$\frac{\Delta\eta}{\eta}$ %
category EE	42	1.2	10
category SS	43	0.49	13
category ES	71	0.52	10

4.3 Analysis using additional measurements

Next, we considered the following cases.

- ANGLE: In this case, the sampling calorimeter is assumed to measure the incident angle of gammas, in addition to the energy and position of gammas.
- TIMING: In this case, the sampling calorimeter is assumed to measure the timing of gammas, in addition to the energy and position of gammas.
- KLONG: In this case, the detector setup is assumed to be able to measure the time of flight of K_L, in addition to the energy and position of gammas.

4.3.1 ANGLE

In this section, in addition to the gamma's energy and hit position in the calorimeter, we assumed that we can measure the incident angle of gammas. Actually, KOPIO experiment is planning to use this technique.

If two gammas come from different pions, the incident angle is usually different from the angle of the line connecting the hit position and the reconstructed vertex. If the detector has a perfect angle resolution, we can remove most of the odd pair background events.

We assumed that the detector can measure incident angle of photons with resolution[8]:

$$\Delta\theta = \frac{0.4\theta + 4.0}{\sqrt{E}}(degree) \tag{4.6}$$

where θ is zenith angle to the surface of the calorimeter of gamma in degree and E is energy of gamma in GeV.

Figure 4.7 shows the difference between the angle using the vertex and the measured incident angle for the 2 photons from $K_L \to \pi^0\nu\bar{\nu}$ and $K_L \to \pi^0\pi^0$ events. In this section, we require that the difference is within 2σ .

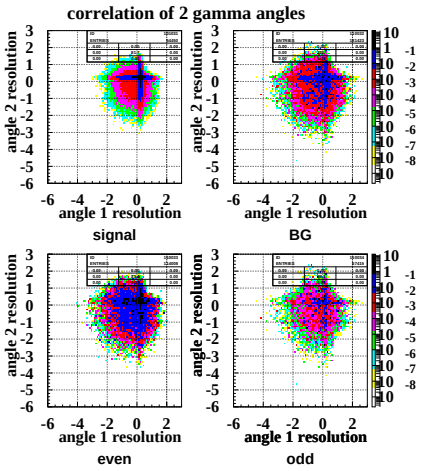

Figure 4.7: angle resolution

Figure 4.8 shows the kinematical signature with the angle cut. We use the same cut region on P_T and Z as Table 4.2. After the cut, we can get the number of signal events, signal to background ratio, and $\frac{\Delta\eta}{\eta}$ for each hit category. The result is shown in Table 4.4.

Table 4.4: The number of signal, signal to background ratio and $\frac{\Delta\eta}{\eta}$ with analysis using only energy and hit position of gammas and the photon angles.

	signal	signal to background ratio	$\frac{\Delta\eta}{\eta}$ %
category EE	40	1.3	10
category SS	42	0.49	13
category ES	69	0.54	10

The error on the weighted average of η is 6.4 %.

Cutting on the photon angle did not improve the signal to background ratio. This is because the angle resolution we assumed in eq.4.6 is too large for photons entering at shallow angles. We should make the detector sensitive to those shallow angle photons.

4.3.2 TIMING

In this section, we assume that in addition to the gamma's energy and hit position in calorimeter, we can measure the timing of gammas.

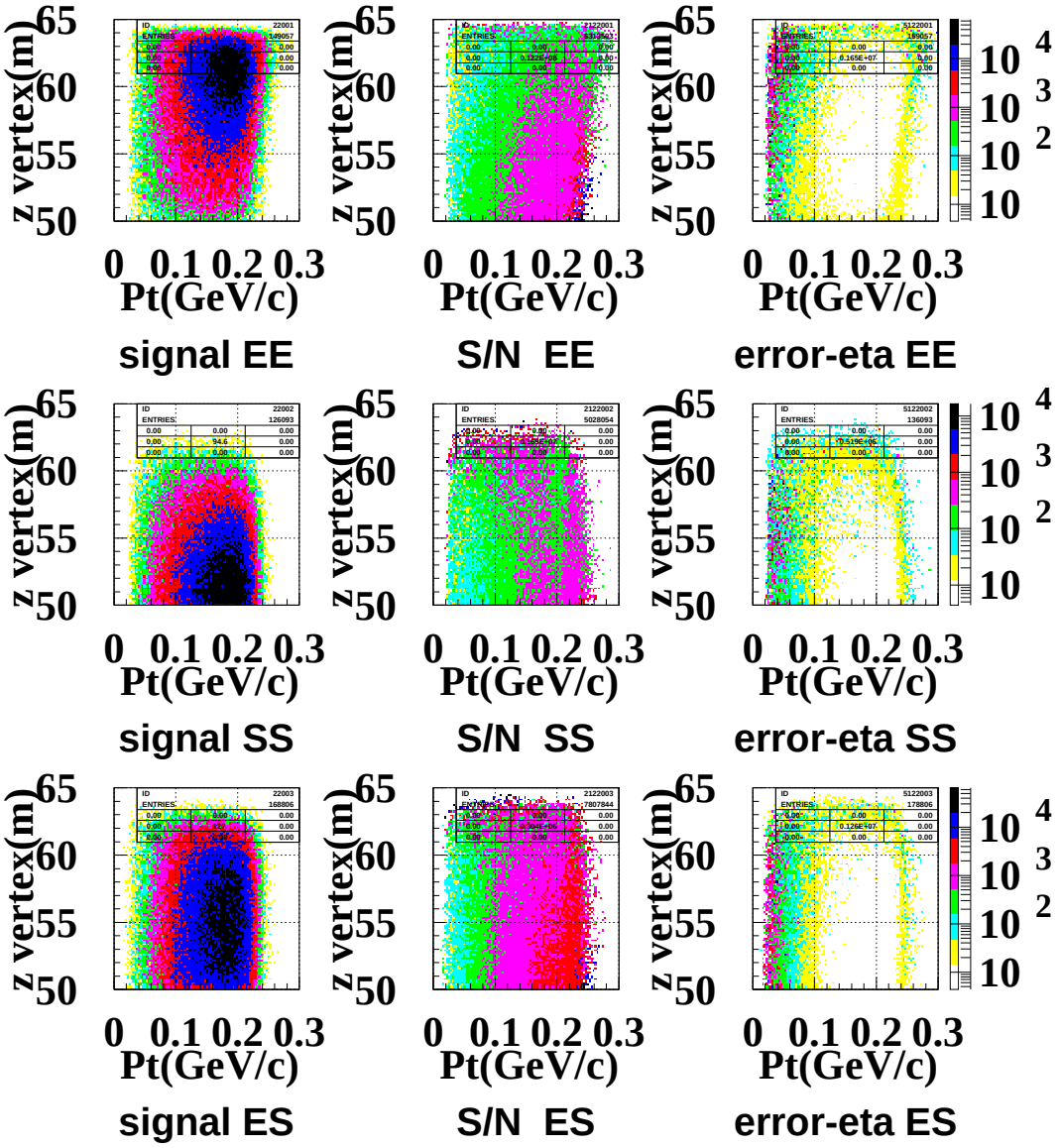

Figure 4.8: kinematical signature with angle

The purpose of measuring the timing is to suppress the odd pair background. We can measure the time difference (ΔT) between two gammas hits timing. Using the distance between the reconstructed vertex and the gammas hit positions, we can calculate the timing difference (ΔT_z) between the two photons. For odd pair background, these can be different, since the reconstructed Z vertex is wrong.

There can be however, two candidate decay positions, typically in the upstream and downstream of the detected position. As mentioned in Section 4.2, we chose the one in the upstream in this simulation.

Here, we assumed a timing resolution[9]:

$$\sigma_T = \frac{50}{\sqrt{E}} + 50(psec) \tag{4.7}$$

where E is the energy of gamma in GeV.

Figure 4.9 shows the distribution of ($\Delta T_z - \Delta T$). We required that ΔT_z and ΔT match within 2σ.

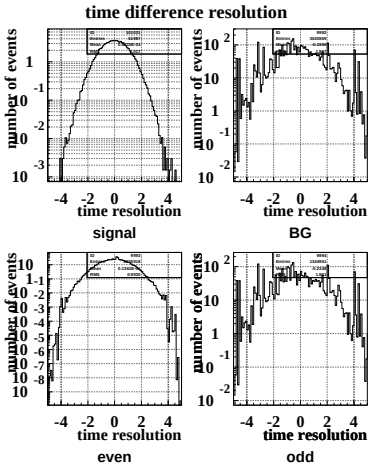

Figure 4.9: timing resolution

Figure 4.10 shows the results of the kinematical signature with the timing cut. We use the same cut region on P_T and Z as shown in Table 4.2. After the cut, we can get the number of signal events, the signal to background ratio and $\frac{\Delta\eta}{\eta}$ for each hit category. The result is shown in Table 4.5. The error on the weighted average of η is 5.7%.

For category EE, the timing did not help because the time difference between 2 gammas at the End Calorimeter is less sensitive to the Z vertex. For category SS or ES, the signal to background ratio is improved by a factor 2.

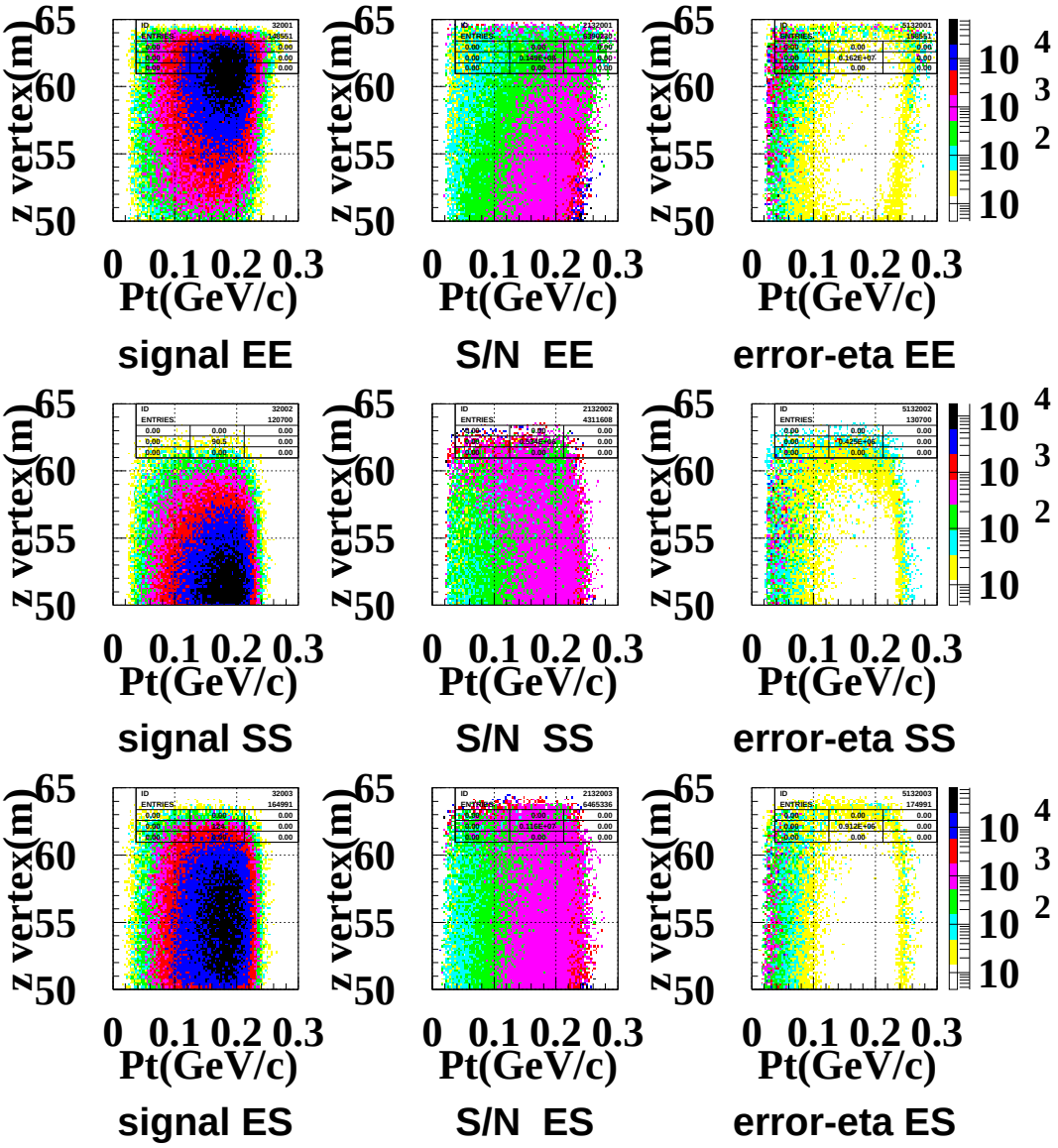

Figure 4.10: cut-criteria 2D plot for timing

Table 4.5: The number of signal events, signal to background ratio and $\frac{\Delta\eta}{\eta}$ with analysis using only energy and hit position of gammas and photons timing

	signal	signal to background ratio	$\frac{\Delta\eta}{\eta}$ %
category EE	39	1.3	11
category SS	41	0.95	11
category ES	68	1.1	8.3

4.3.3 KLONG

In this section, we assumed that in addition to the gamma's energy and hit position in the calorimeter, we can measure the TOF of K_L as KOPIO experiment.

In this case, the aim is to suppress the even pair backgrounds. With K_L TOF, we can calculate missing mass, which is the invariant mass of the unobserbed particles. Assuming that the two observed gammas come from one pion, the missing energy is written as,

$$M^2_{miss} \equiv (E_{K_L} - E_{\gamma\gamma})^2 - (\overrightarrow{\mathrm{P_{K_L}}} - \overrightarrow{\mathrm{P}_{\gamma\gamma}})^2 \tag{4.8}$$

$$= M^2_{K_L} + M^2_{\pi^0} - 2E_{K_L}E_{\gamma\gamma} + 2P_{zK_L}P_{z\gamma\gamma} \tag{4.9}$$

where E_{K_L} and $E_{\gamma\gamma}$ are the energies of K_L and two observed gammas, $\overrightarrow{\mathrm{P_{K_L}}}$ and $\overrightarrow{\mathrm{P}_{\gamma\gamma}}$ are momentum of K_L and two observed gammas, M_{K_L} and M_{π^0} are the mass of K_L and π^0, and, P_{zK_L} and $P_{z\gamma\gamma}$ are Z component of the momentum of K_L and two gammas. Here, we assumed that K_L's came along the Z axis. In the case of even pair background, missing mass should be a pion's mass, so we can cut events around the pion's mass. If the detector has a perfect resolution, M^2_{miss} corresponds to $M^2_{\pi^0}$, that is, 18220 $(\mathrm{MeV/c^2})^2$.

Here, we assumed that the resolution of TOF was 500psec, governed by an assumed the bunch width of protons.

Figure 4.11 shows the missing mass distribution. We required the missing mass to have

$$(M_{\pi^0} - 20MeV/c^2)^2 \leq M^2_{miss} \leq (M_{\pi^0} - 20MeV/c^2)^2 \tag{4.10}$$

Figure 4.12 shows the kinematical signature with the TOF cut.

The K_L TOF did not improve the sensitivity. If we want to use missing mass cut with our high K_L momentum, the resolution of TOF should be smaller.

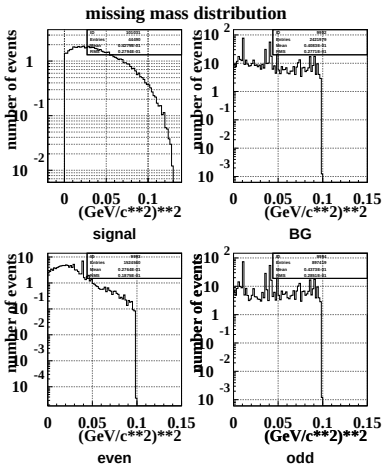

Figure 4.11: missing mass distribution

Table 4.6: The number of signal events, signal to background ratio and $\frac{\Delta\eta}{\eta}$ with analysis using only energy and hit position of gammas and the TOF of K_L.

	signal	signal to background ratio	$\frac{\Delta\eta}{\eta}$ %
category EE	38	1.26	0.11
category SS	36	0.49	0.15
category ES	62	0.50	0.11

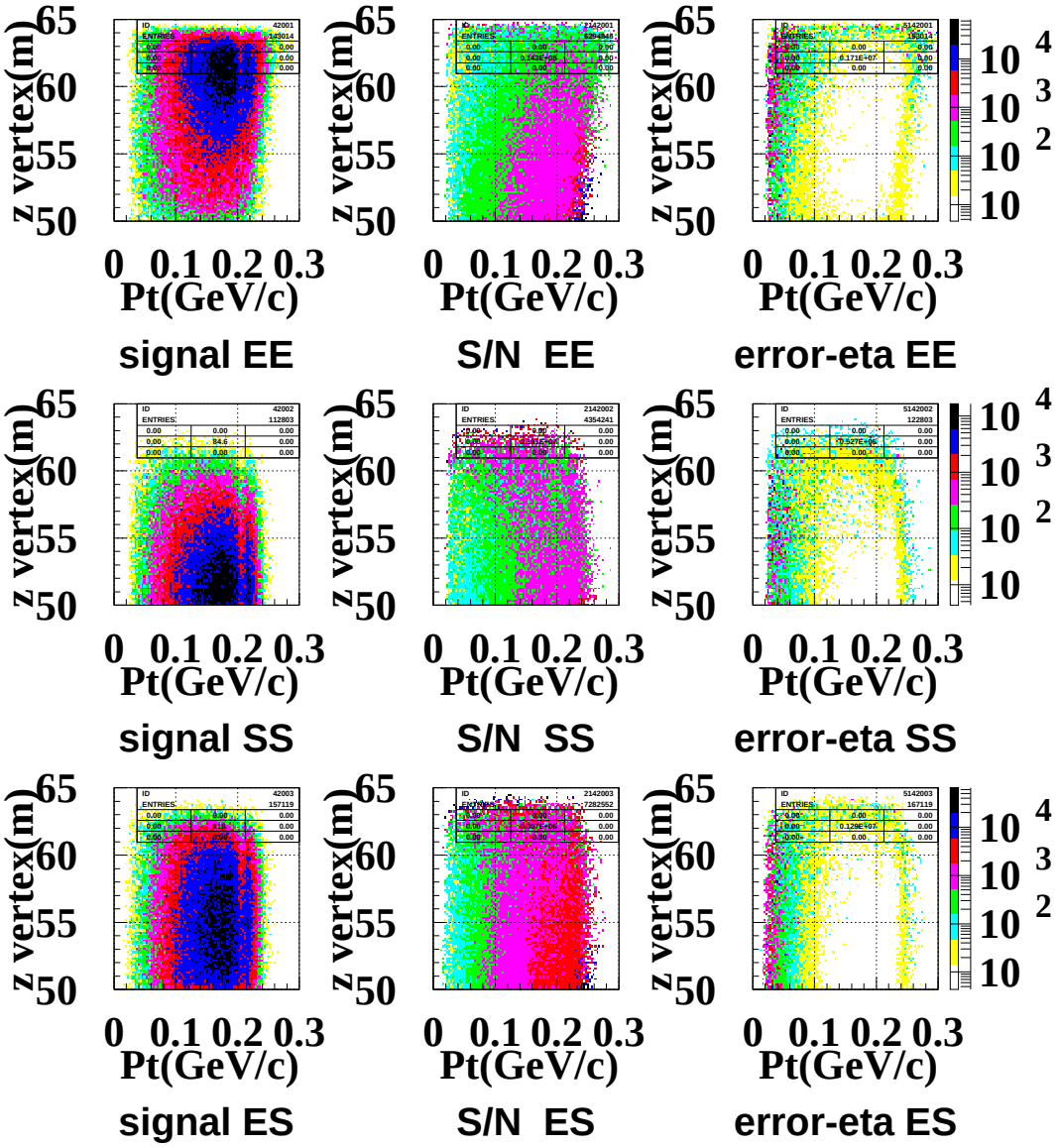

Figure 4.12: cut-criteria 2D plot for TOF

4.4 Summary

Using only energy and hit position of gammas, and with 3×10^{20} protons on target, we can measure η to 6.4 % of itself by collecting 156 signal events with the signal to background ratio 0.6. If we apply a cut on the timing difference between the 2 photons, the signal to background ratio is improved to 1.1, while keeping 148 signal events. The error on η is 5.7% of itself.

Chapter 5

Improvement on the detector

In order to suppress the number of background events, we have studied two conditions. One is lower energy threshold for vetoing photons and second is better angle resolution.

5.1 A Veto threshold

We lowered the photon veto threshold from 5 MeV to 2 MeV. The new inefficiency is shown in Fig 5.1.

Figure 5.2 shows the kinematical signature with 2 MeV threshold. Only energy and hit position of gammas were used in the analysis.

After applying the cut as shown in Table 4.2, we obtained the number of the signal events, the signal to background ratio, and $\frac{\Delta\eta}{\eta}$ for each hit category as shown in Table 5.1. Similarly, if we applied the additional cut on the timing difference between the two photons, we obtained the result shown in 5.2.

The error on the weighted average of $\frac{\Delta\eta}{\eta}$ is 4.9% for analysis using only energy and hit position of gammas, and 4.7% with the additional timing cut. In addition, the signal to background ratio is 2.0 for analsis using only energy and hit position of gammas, and 3.4 with the additional timing cut.

Table 5.1: The number of signal events, signal to background ratio and $\frac{\Delta\eta}{\eta}$ with analysis using only energy and hit position of gammas.

	signal	signal to background ratio	$\frac{\Delta\eta}{\eta}$ (%)
category EE	41	3.7	8.8
category SS	42	1.4	10.1
category ES	71	2.1	7.2

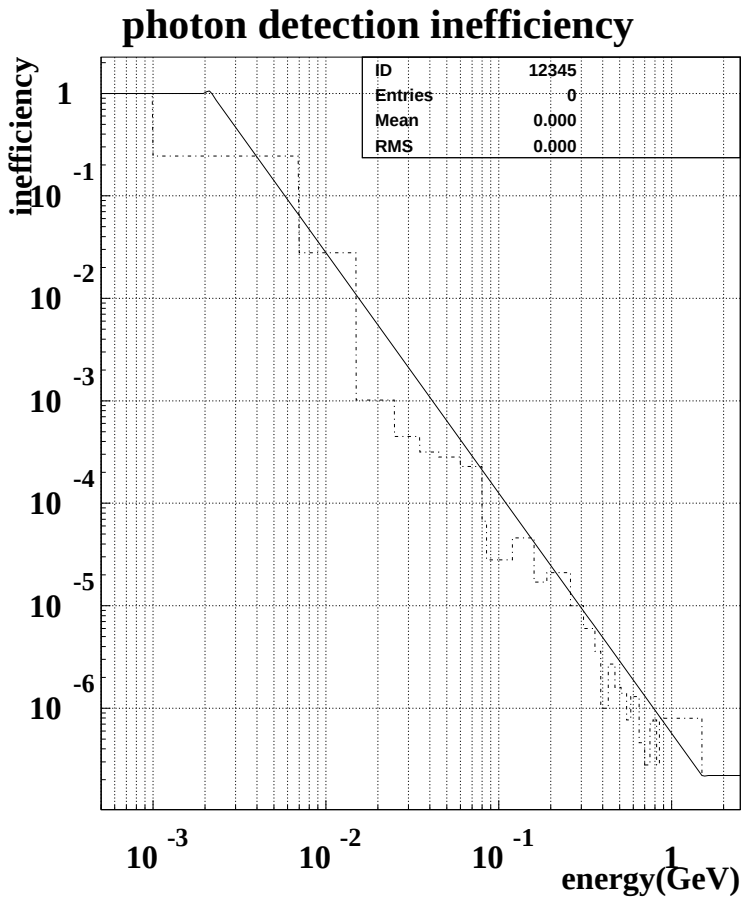

Figure 5.1: Photon detection inefficiency as a function of the photon energy for 1mm Pb/5mm Scintillator sampling calorimeters whose threshold is 5MeV. The dotted line is experimental data [7]. The solid line shows the inefficiency we assumed in the simulation.

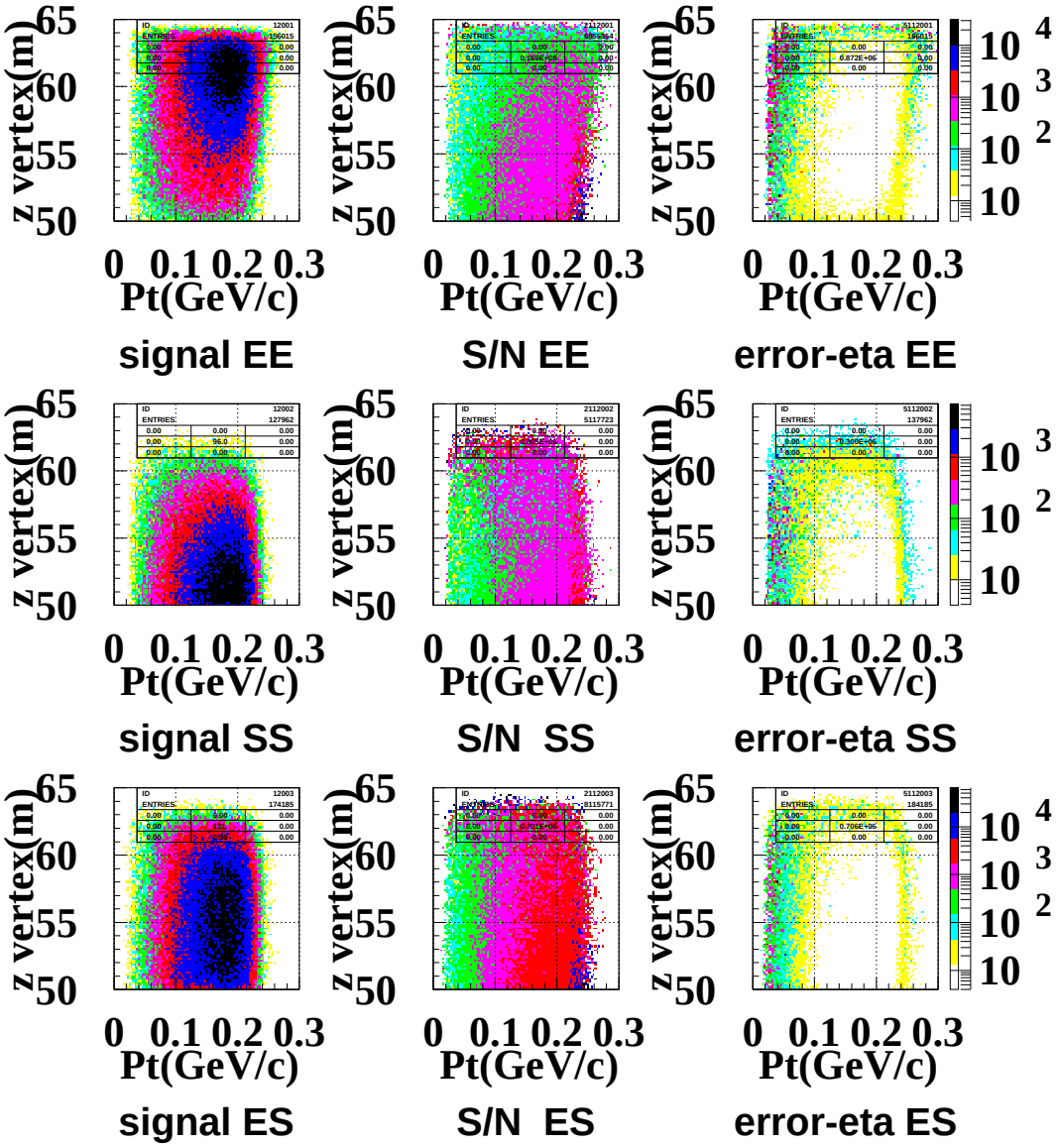

Figure 5.2: kinematical signature with 2 MeV threshold energy

Table 5.2: The number of signal events, signal to background ratio and $\frac{\Delta\eta}{\eta}$ with additional timing.

	signal	signal to background ratio	$\frac{\Delta\eta}{\eta}$ (%)
category EE	39	3.8	9.0
category SS	40	3.3	9.0
category ES	67	3.2	7.0

5.2 Angle resolution

In section 4.3.1, We assumed that the detector can measure incident angle of photons with resolution eq. 4.6. But this angle resolution is not effective for suppressing background with photons entering at shallow angles. In this section, we assumed that the angle resolution is independent of the incident angle:

$$\Delta\theta = \frac{4.0}{\sqrt{E}}(degree) \tag{5.1}$$

where E is energy of gamma in GeV.

After applying the same cut as shown in section 4.3.1, we obtained the number of the signal events, the signal to background ratio, and $\frac{\Delta\eta}{\eta}$ for each hit category as shown in Table 5.3.

The error on the weighted average of $\frac{\Delta\eta}{\eta}$ is 5.9%. This value differs from the value of timing cut in section 4.3.2 by 0.2%. This is because angle or timing cut can suppress odd pair backgrounds. For category EE, the angle cut did not help because the difference between the angle using the vertex and the measured incident angle fades away. For category SS or ES, the signal to background ratio is improved by a factor 1.7 or 1.6 compared to with the former angle resolution in section 4.3.1.

Table 5.3: The number of signal, signal to background ratio and $\frac{\Delta\eta}{\eta}$ with analysis using only energy and hit position of gammas and the photon angles.

	signal	signal to background ratio	$\frac{\Delta\eta}{\eta}$ %
category EE	39	1.4	11
category SS	39	0.83	12
category ES	67	0.84	9.1

Chapter 6

Conclusion

Using the 'Side Calorimeter' we can get the signal events by factor 3.7 compared to the 'End Calorimeter' only. By requiring the time difference between 2 gammas to be consistent with their reconstructs path length, the signal to background ratio is improved from 0.6 to 1.1. We found that we can collect more than 148 events in 3 years of running at 10% of the full accelerator intensity. The signal to background ratio is 1.1 with the photon veto threshold set at 5 MeV. With this statistics, we can measure η to within 6%. If we lower the photon veto threshold to 2 MeV, the signal to background ratio is improved to 3.4, and the error of η is reduced to 4.7%.

Bibliography

[1] J. Cronin, V. Fitch *et al.*, Phys. Rev. Lett. **13**, 138 (1964).

[2] M. Kobayashi and T. Maskawa, Prog. Theor. Phys. **49**, 652 (1973).

[3] L. Wolfenstein, Phys. Rev. Lett. **51**, 1945 (1983).

[4] A. Buras, Phys. Lett. **B333**, 476 (1994).

[5] G. Buchalla and A. Buras, Phys. Rev. **D54**, 6782 (1996).

[6] A. Alavi-Harati *et al.*, Phys. Rev. **D61**, 072006 (2000).

[7] K.Manabe, Master Thesis, Osaka Univ., "Bottom Up Study of $K_L \to \pi^0 \nu\bar{\nu}$ experiment", (2000)

[8] Y. Shibata, Private communication.

[9] I-H. Chiang *et al.* (KOPIO Collaboration), "KOPIO - A study of Klong -¿ pi0 nu nubar", (1999)